Coupled Electromagnetic Treatment Enhancing Magnetic Performance of Mn-Zn Power Ferrites for Power Electronics Applications

Yuan Wang [a], Shiyuan Zhang [a], Bo Zeng [a], Kunlan Huang [a,*], Yi Qin [b], Jie Wang [a]

[a] *School of Mechanical Engineering, Sichuan University, Chengdu, Sichuan 610065, P.R. China*

[b] *Centre for Precision Manufacturing, DMEM, The University of Strathclyde, James Weir Building, 75 Montrose Street, Glasgow G1 1XJ, UK*

(*) Corresponding Author: Kunlan Huang, E-Mail: huangkunlan@scu.edu.cn.

Abstract

In this work, a coupled electromagnetic treatment (CEMT) was proposed to enhance the magnetic performance of Mn-Zn power ferrites, addressing the increasing demand for functionality and efficiency in soft magnetic materials. This study investigates the effects of CEMT on the initial permeability and power loss of EP-13 Mn-Zn ferrite cores through systematic experimental analysis. The optimal CEMT conditions were identified as a magnetic field intensity of 1.5T, an electric field intensity of 1V, and 20 magnetization cycles. Under these conditions, the initial permeability increased by 10.09% at 25°C and by 5.58% at 100°C. The power loss was reduced by 2.80% at 25°C and by 6.81% at 100°C, while the coercivity was reduced by 19.51%, and the saturation magnetization increased by 4.63%. Further microstructural analysis revealed that CEMT effectively promoted the transformation of low-angle to high-angle grain boundaries, facilitated dislocation rearrangement and annihilation, and contributed to residual stress relaxation. A reduction in microstructural defects was also observed at the grain boundaries. These changes reduced domain wall pinning and improved domain wall mobility, resulting in lower power loss. In summary, the results demonstrate that CEMT is an effective and environmentally friendly technique for optimizing the microstructure and magnetic properties of Mn-Zn ferrites. This method offers a promising strategy for improving initial permeability and reducing power loss in high-performance power ferrite applications, while also demonstrating the flexibility and scalability of CEMT for future industrial use.

Keywords: Mn-Zn power ferrites, Electromagnetic properties, Coupled electromagnetic treatment, Microstructure

1. Introduction

Mn-Zn power ferrite is an important soft magnetic material that plays a crucial role in the efficient operation of modern power electronics and electrical machines. Due to its excellent properties, including high saturation magnetization, high initial permeability, high chemical stability, and low power loss, it is widely used as a core material in electronic devices such as transformers, converters, inverters, magneto-fluidic devices, and gas sensors [1]. The advancement of power electronics toward

miniaturization, lightweight design, and high efficiency has imposed increasingly stringent requirements on the magnetic properties and loss characteristics of Mn-Zn ferrite [2-4]. Among these properties, initial permeability (μ_i) and power loss (P_c) are the most critical performance indicators [5]. For instance, in electric motor applications within the transportation sector, where energy storage is limited, stringent requirements for high efficiency and low power loss must be met. Mn-Zn ferrite cores are typically used in alternating magnetic field environments, where magnetic losses generated during dynamic magnetization significantly impact their performance. Excessive magnetic losses not only result in energy waste but also lead to material heating and permeability dispersion, ultimately affecting the long-term stability and operational reliability of ferrite components [6,7]. Additionally, under identical operational conditions, ferrite cores with higher initial permeability require fewer coil windings, thereby reducing the overall size of components, optimizing material usage, and lowering manufacturing costs, which enhances the overall economic efficiency of the system.

Recently, reducing magnetic losses, improving the initial permeability of ferrite cores, and enhancing material stability under high-frequency and varying temperature conditions have become major research objectives in the field of soft magnetic materials. Researchers have proposed various optimization strategies for different production stages of Mn-Zn power ferrites, which can be generally divided into elemental doping and process optimization [5,8]. Among these strategies, doping with additional elements or oxides (such as Y_2O_3, HfO_2, Bi_2O_3, and Co_2O_3) can optimize the microstructure and adjust magnetic anisotropy, thereby reducing magnetic losses and improving permeability [9-11]. For example, Zaspalis et al. [12] found that doping Nb_2O_5 into pure Mn-Zn ferrite significantly reduced total power loss per unit volume, particularly those associated with magnetostriction and stress-induced hysteresis. Similarly, Ji et al. [13] reported that Cr-Mg co-doping in NiCuZn ferrites effectively enhances their magnetic performance, such as high permeability, high saturation magnetization, and low coercivity, demonstrating promising potential for applications in magnetic hyperthermia. Furthermore, the increase in electrical resistivity led to a reduction in eddy current losses, further optimizing the material's performance. Additionally, modifying sintering parameters, including temperature, pressure, and atmospheric conditions, can refine grain size and improve grain boundary

characteristics, further enhancing magnetic performance [14]. Ying et al. [15] used a cold sintering process to produce Mn-Zn ferrites with a relative density of 85.4% and smaller grain sizes, achieving a notable reduction in power loss.

Despite the progress made in improving the magnetic properties of Mn-Zn ferrites, most existing methods require modifications to the original manufacturing process, leading to increased production costs, greater energy consumption, and challenges in process control. Moreover, the microstructural defects introduced during the doping process may compromise the long-term stability of the material's magnetic performance [16]. Current research has devoted limited attention to the role of non-doping techniques in optimizing the magnetic properties of Mn-Zn ferrites. Therefore, it is an important challenge to further enhance the magnetic performance of Mn-Zn ferrites through material processing techniques without altering their chemical composition.

The past few years have seen extensive use of electromagnetic field treatment technology for material modification, which includes microstructural refinement, stress relief, and grain refinement [17]. Klameck [18] demonstrated that magnetic fields can induce dislocation motion and rearranged dislocation structures. As the magnetic field intensity varies, alternating magnetostriction within the sample generates internal magnetic vibrations, leading to the formation of distributed microplastic strain, which subsequently influences the material's microstructure. Pan et al. [19] reported that pulsed current can generate a driving force for dislocations, facilitating their migration and ultimately inducing microplastic deformation within the material. Furthermore, M. N. Shipko et al. [20] investigated the effects of pulsed magnetic fields on the crystal structure and macroscopic magnetic properties of hexagonal barium ferrites. They found that pulsed magnetic treatment can modify the defect structure within the crystal lattice, thereby influencing magnetic performance. These findings show that using electromagnetic fields during processing has many benefits, like fixing small defects and reducing leftover stress in materials, all while keeping the original size and surface shape of the parts unchanged. Additionally, through the research conducted by Cai et al. [21], it can be observed that compared to single-pulse field treatment, coupled electromagnetic treatment (CEMT) demonstrates a more pronounced effect in enhancing material performance and reducing residual stress. This is because, during the treatment, the magnetic field and electric field act synergistically to provide driving

force for dislocation movement, rearranging and uniformly distributing dislocations entangled at grain boundaries and defects throughout the crystal. This comprehensive effect of simultaneous time and space coupling fundamentally distinguishes CEMT from traditional pulse magnetic field-induced magnetostrictive strain or pulse current heating [22-25].

Compared with traditional strategies such as elemental doping and cold sintering, which often require permanent compositional changes or complex processing conditions, the CEMT offers a non-invasive and low-temperature approach to tailoring microstructure and magnetic behavior. Moreover, this technique incurs no substantial additional economic costs or time constraints, making it a promising approach for material enhancement. The duration of the coupled electromagnetic treatment is only 3-10 minutes, which significantly shortens the processing time compared to conventional modification techniques [23,26].

This study aims to investigate the effect of coupled electromagnetic treatment (CEMT) on key magnetic properties of Mn-Zn ferrite, including magnetic loss and initial permeability. We can identify optimal CEMT parameters by comparing the magnetic performance of specimens under different parameters. Furthermore, we will examine the microstructural evolution of Mn-Zn ferrite components before and after processing under the optimal CEMT parameters to elucidate the underlying mechanisms contributing to the improvement in magnetic performance.

2. Experimental procedure

2.1 Materials

The experimental material used in this study were EP-13 Mn-Zn ferrites with external dimensions of 12.5×9.5×9mm and Φ4.5mm (inner cylinder), as shown in Fig. 1(b). The EP-13 Mn-Zn ferrite cores used in this study were supplied by Yibin Yingtai Optoelectronics Co., Ltd (China). The raw materials used in the production had a purity of no less than 99.5%, including iron oxide (Fe_2O_3), manganese tetroxide (Mn_3O_4) and zinc oxide (ZnO). The chemical composition of the tested Mn-Zn ferrites is listed in Table 1. The manufacturing process of Mn-Zn ferrites includes ball milling, pre-firing, secondary ball milling after adding an appropriate number of additives, granulation, pressing, and sintering. All the ferrites used in the study were commercial products.

Table 1 Chemical composition of Mn-Zn ferrite

Composition	Mn	Zn	K	Co	Sn	Fe
Wt.%	24.10	7.60	0.30	0.12	0.06	67.82

2.2 Coupled electromagnetic treatment experiments

The CEMT experiments were conducted using a CEMT experimental platform independently designed and customized by Sichuan University. The CEMT experiment platform consists of an electric and magnetic field generating unit, a PLC control unit, and a power capacitor. The electromagnetic field processing unit comprises two copper electrodes and a ring-shaped excitation coil. The sample is placed between the copper electrodes, which are connected to the power source to generate pulsed electric fields. The ring-shaped excitation coil is connected to the capacitor, and when the capacitor is charged and discharged, pulsed currents flowing through the excitation coil generate pulsed magnetic fields in the cavity space. The magnetic field intensity ranges from 0 to 2.5T. Pulsed currents are supplied by the power source, converting 380V/50Hz industrial AC power to DC power, with a maximum current of 5000A, voltage range of 0-10V, and an adjustable pulse frequency. The PLC control unit synchronously operates the current power supply and the excitation coil power supply to create different spatial fields (single electric field, single magnetic field, coupled electromagnetic field) within the cavity. Fig. 1 depicts a schematic diagram of the CEMT device used in this experiment. The entire process was conducted at room temperature and standard atmospheric pressure, achieving different treatments of manganese zinc ferrite: electric treatment (CT), magnetic treatment (MT), and coupled electromagnetic treatment (CEMT). The CEMT experimental processing parameters for the specimens in this study are presented in Table 2. In this study, the ranges of electric and magnetic field parameters were determined through a comprehensive consideration of prior experimental reports, COMSOL simulation results, and the performance range of our equipment. Previous studies have shown that an electric field in the range of 1V-1.2V and a magnetic field in the range of 1-1.5T are sufficient to effectively drive dislocation motion, promote dislocation rearrangement and annihilation, and activate magnetostrictive strain, thereby improving microstructural and magnetic properties [27,28]. Accordingly, we conducted gradient experiments with pulsed electric fields from 0 to 1.5V and magnetic fields from 0 to 2T. The magnetic field was not set beyond 2T because excessively strong fields induced severe vibrations during treatment, which

risked mechanical damage to the fragile ferrite specimens. We limited the maximum pulsed electric field to 1.5V because Mn-Zn ferrites have extremely low electrical conductivity, and COMSOL simulations further confirmed that voltages above this threshold produced negligible changes in the internal field distribution. This parameter design ensures coverage of the optimal treatment window suggested by literature while maintaining compatibility with our device performance and industrial feasibility.

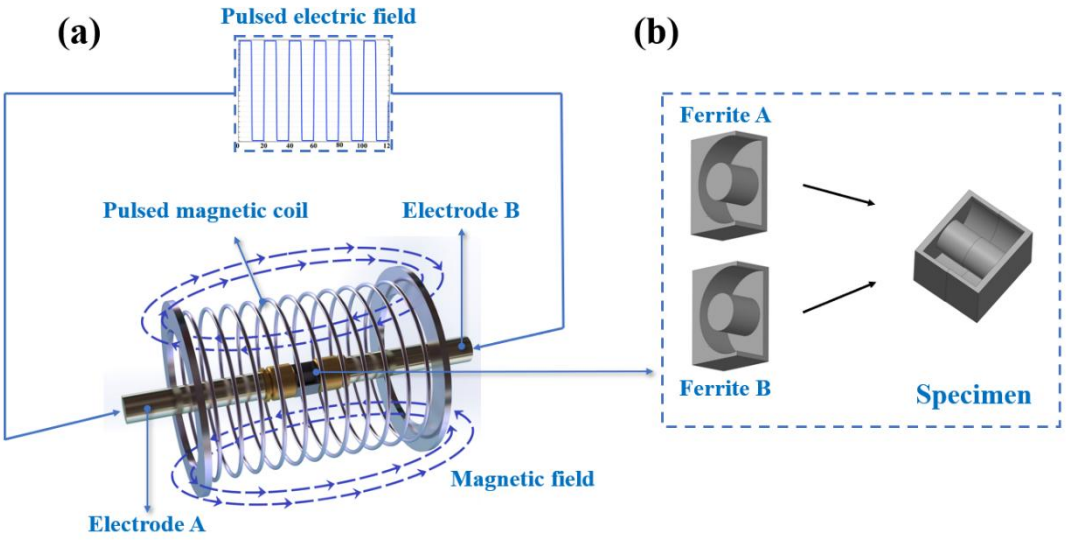

Fig. 1 Illustration of the experimental process: (a) schematic diagram of CEMT process, (b) schematic diagram of specimen clamping

Table 2 CEMT processing parameters.

Treatment	Sample number								
	#0	#1	#2	#3	#4	#5	#6	#7	#8
Electric field intensity (V)	0	1	1	1	1	1	0	0.5	1.5
Magnetic field intensity (T)	0	0	0.5	1	1.5	2	1.5	1.5	1.5

2.3 Magnetic performance test and microstructure observation

The magnetic core loss and initial permeability of Mn-Zn ferrite subjected to different CEMT were measured using the SY-8232 B-H analyzer under 100kHz and 200mT with temperature at 25℃ and 100℃. All specimens were taken from the same production batch of EP-13 Mn-Zn ferrites, and for each condition, three independent samples with similar initial properties were tested. The power loss of the optimally parameter-treated sample, which exhibited the most significant improvement in magnetic properties, as well as the untreated sample, was measured over a wide temperature range from 25℃ to 125℃, with measurements taken at 25℃ intervals.

During the testing process, measurements were conducted sequentially from low to high temperatures. After each lower-temperature measurement was completed, the sample was heated to the next set temperature, followed by a stabilization period before performing the high-temperature measurement. The initial magnetization and hysteresis loop data of Mn-Zn ferrite core samples were measured under a magnetic field range of -2T to +2T at room temperature (25℃) using a Quantum Design PPMS comprehensive physical property analyzer.

The structural characterization of the samples was performed by X-Ray diffraction (XRD) using X'pert Pro-P Analytical instrument (Cu-Kα X-Rays). The surface and fracture surface microstructure of Mn-Zn ferrites were examined using a field emission scanning electron microscope (Thermo Scientific ApreoSe USA). The elemental composition at the grain boundaries was analyzed using energy dispersive spectroscopy (EDS). The quasi-in-situ EBSD of Mn-Zn ferrite specimen before and after the CEMT was performed using a JSM7200F field emission SEM fitted with an EDAX EBSD Velocity detector. The specific experimental steps were as follows: (1) Select the upper surface of the central cylindrical region of the EP-13 specimen as the observation surface. Use an IM4000II ion milling system for planar argon ion polishing. Perform EBSD scanning with a step size of 1μm over an area of 402×402 μm^2. Locate the observation surface and record the data, (2) Subject the specimen to CEMT, (3) Reposition the scan area based on micro-indentation, perform EBSD scanning at the same collection step size, and record the data, (4) Compare the EBSD results in the same micro-region of the specimen before and after CEMT and analyze them using HKL CHANNEL5 software.

3. Results and discussion

3.1 Electromagnetic properties

As shown in Fig. 2(a)-(d), the initial permeability (μ_i) of EP-13 Mn-Zn ferrite is relatively high, and it exhibits varying changes after CEMT processing. Each data point represents the mean value of three independent samples, with error bars indicating standard deviation. With a fixed electric field of 1V, the enhancement in the initial permeability of EP-13 Mn-Zn ferrite initially increases and subsequently decreases as the pulsed magnetic field strength rises. At 25°C, the most pronounced enhancements are observed under pulsed magnetic field parameters of 0.5T and 1.5T, with increases of 2.04% and 10.09%, respectively. At 100°C, the initial permeability increases by 5.58% under the 1.5T condition, while changes under other magnetic field parameters are negligible. Furthermore, with a fixed magnetic field of 1.5T, the effect of increasing the electric field on the initial permeability at both 25°C and 100°C exhibits a similar trend. The most significant improvement is observed at 1V, resulting in enhancements of 10.09% at 25°C and 5.58% at 100°C.

Generally, manganese-zinc ferrite is required to have a high permeability. In practical applications, the permeability typically used is the initial permeability (μ_i), which represents a macroscopic physical quantity describing the magnetization process of manganese-zinc ferrite after it has been demagnetized in a weak magnetic field. Its specific definition is given by the following equation:

$$u_i = \frac{1}{u_0} \lim_{\Delta H \to 0} \frac{\Delta B}{\Delta H} = \frac{1}{u_0} \left[\frac{dB}{dH}\right]_{H=0} \quad (1)$$

ere u_0 is the vacuum magnetic permeability, and B is the magnetic induction intensity, and H is the external magnetic field intensity.

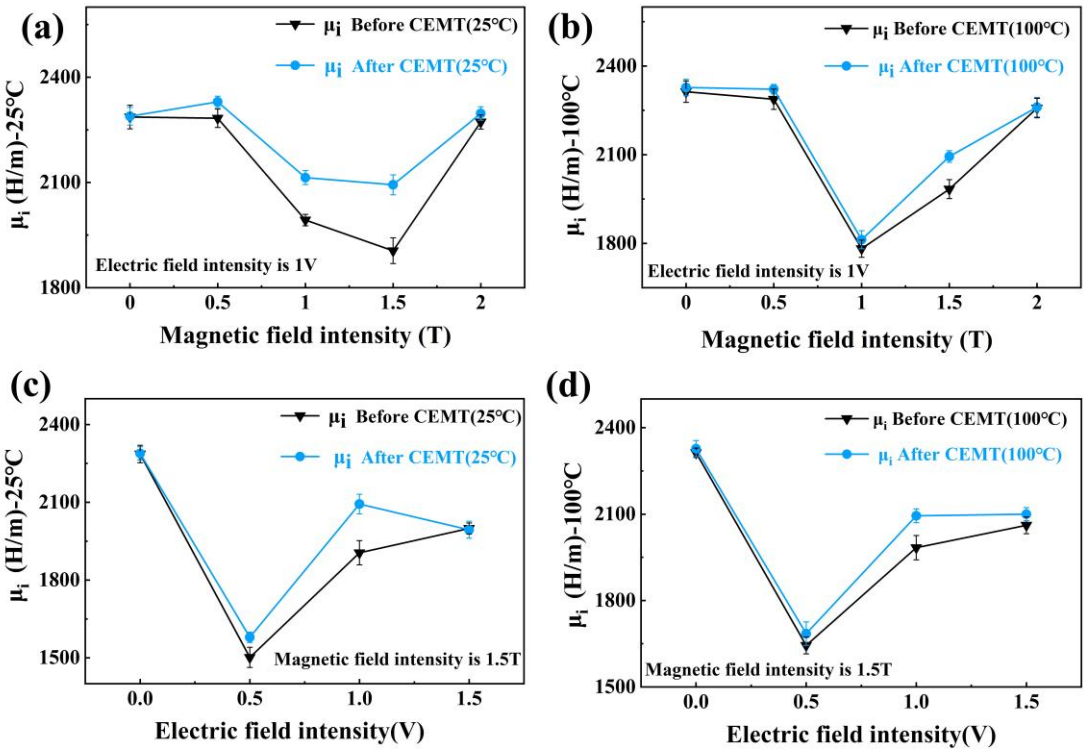

Fig. 2 Effect of CEMT on initial permeability (μ_i) of magnetic properties: (a) effect of magnetic field parameters on initial permeability at 25°C, (b) effect of magnetic field parameters on initial permeability at 100°C, (c) effect of electric field parameters on initial permeability at 25°C, (d) effect of electric field parameters on initial permeability at 100°C.

Following CEMT processing, the power loss of EP-13 Mn-Zn ferrite is reduced. As shown in Figs. 3(a) and (b), with a fixed electric field of 1V, power loss is significantly decreased at 25°C under various pulsed magnetic field parameters, with the largest reduction of 2.80% observed at 1.5T. At 100°C, the most pronounced decline in power loss occurs at 1.5T, with a reduction of 6.81%, while power loss remains nearly unchanged at other magnetic field conditions. Additionally, Fig. 3(c) and (d) reveal that, under a fixed magnetic field of 1.5T, power loss decreases noticeably with increasing electric field. At 25°C, significant reductions are observed at electric fields of 1V and 1.5V, with the largest reduction of 2.80% occurring at 1.5V. At 100°C, marked reductions in power loss occur at electric fields of 0.5V and 1V, with the maximum reduction of 6.81% seen at 1V, while power loss remains largely unchanged at 1.5V.

The differences in magnetic performance improvement under different electromagnetic parameters are primarily due to the varying degrees of microstructural refinement induced by the electromagnetic treatment. At lower magnetic and electric field intensities, the magnetostriction effects and dislocation activation are weak, and

the energy provided by the electromagnetic field is insufficient to drive significant microstructural changes, resulting in limited improvement in magnetic properties. As the magnetic field strength increases, the synergistic effect of pulsed currents and magnetic fields becomes more effective in promoting dislocation slip and climb, transforming low-angle grain boundaries into high-angle ones, and relieving residual stress. These changes help reduce domain wall pinning and enhance domain wall mobility, thereby improving initial permeability and reducing power loss. However, it is worth noting that the stress induced by magnetostriction effects is non-uniform [7], and studies have shown that the influence of electric fields on dislocation motion is nonlinear [29]. When the field intensity becomes too high, excessive magnetostriction deformation may lead to microplasticity and the formation of new defects, which can offset the magnetic performance gains. Therefore, there exists an optimal range of electromagnetic parameters that balances microstructural enhancement with structural stability, maximizing improvements in magnetic properties.

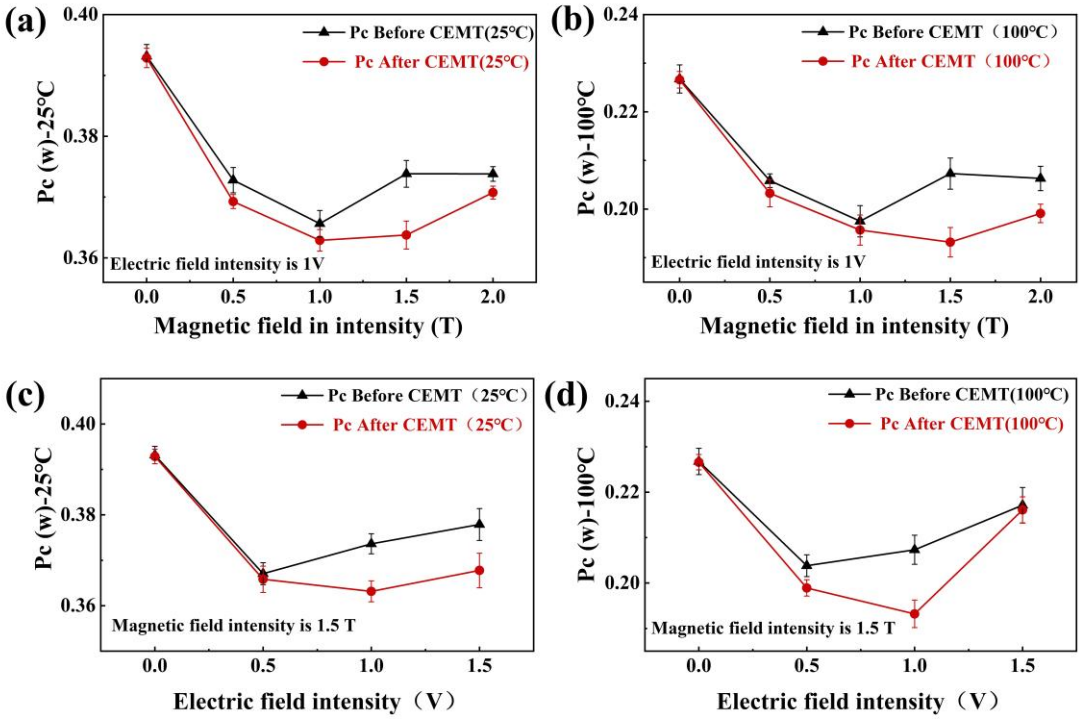

Fig. 3 Effect of CEMT on power losses (P_c) of magnetic properties: (a) effect of magnetic field parameters on power losses at 25°C, (b) effect of magnetic field parameters on power losses at 100°C, (c) effect of electric field parameters on power losses at 25°C, (d) effect of electric field parameters on power losses at 100°C.

For manganese-zinc ferrite, the initial permeability and power loss are two very important parameters. The effect of CEMT on its magnetic performance needs to

consider both factors comprehensively. Among the set parameter gradient groups, the optimal CEMT parameters for electric field and magnetic field were 1V and 1.5T.

Since ferrite cores are often operated at a high temperature range from 80 to 100°C, temperature characteristics of core losses are of critical importance. Namely, for Mn-Zn power ferrites, not only core losses at room temperature but also core losses at the high temperature range are vital to the stability and reliability of entire power transfer components [6]. Power loss tests were conducted on the untreated sample (#0) and the sample (#4) treated with optimal parameters (1V, 1.5T) over a wide temperature range from 25°C to 125°C at 100kHz and 200mT. The results are presented in Fig. 4. It can be observed that after treatment with optimal parameters, the power loss of the sample is reduced across a wide temperature range compared to the untreated sample. Generally, the core power losses (P_c) are composed of three loss factors, namely hysteresis loss P_h, eddy current loss P_e, and residual loss P_r [30]. The eddy current phenomenon caused by the alternating current is the eddy current loss (P_e), the hysteresis phenomenon caused by the magnetic core under the alternating magnetic field is the hysteresis loss (P_h), and the residual loss caused by other factors is the residual loss (P_r). The P_c can be described as the following equation:

$$P_c=P_e+P_h+P_r \quad (2)$$

The resistivity of manganese-zinc ferrites decreases exponentially with increasing temperature, which means that the electrical conductivity increases exponentially with rising temperature. Consequently, when the temperature exceeds 100°C, it can be observed that the power loss begins to exhibit an increasing trend again. This is because the effect of eddy current losses (P_e) on the core losses becomes greater when the conductivity increases and hence the power consumption increases.

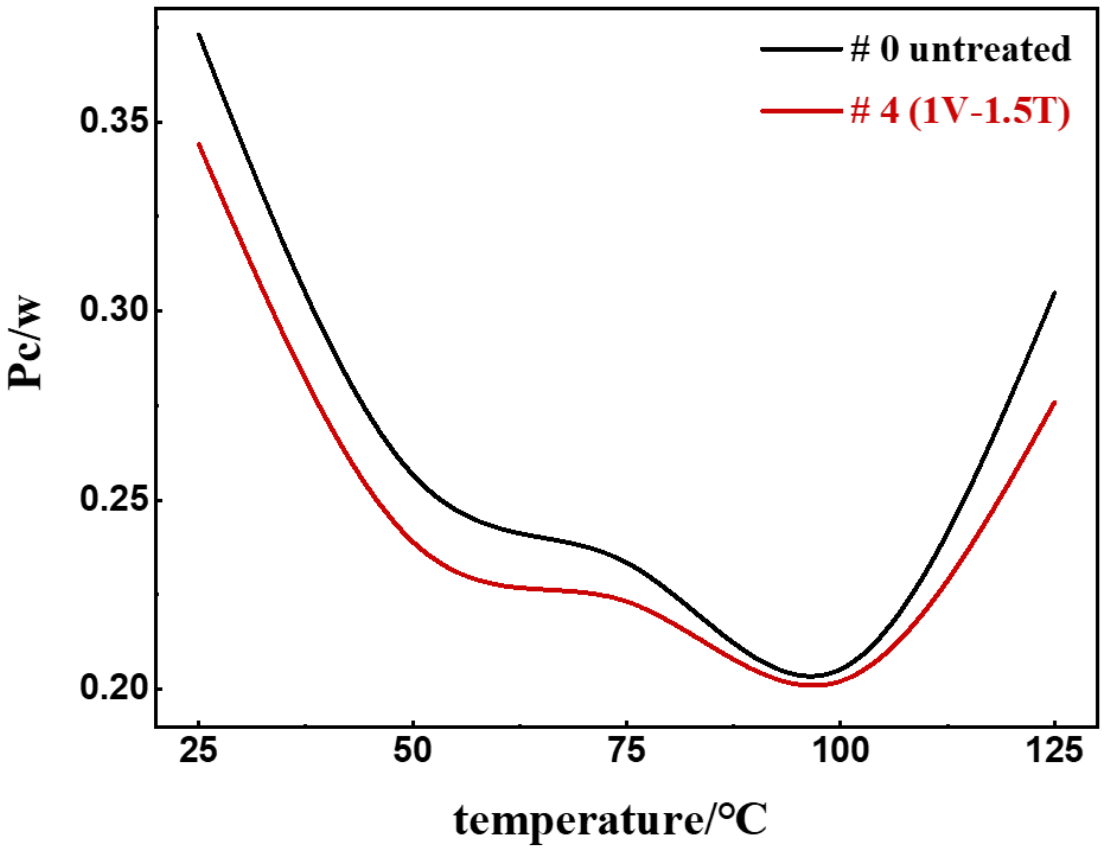

Fig. 4 Power dissipation curve of Mn-Zn ferrite over a wide temperature range pattern of samples after CEMT

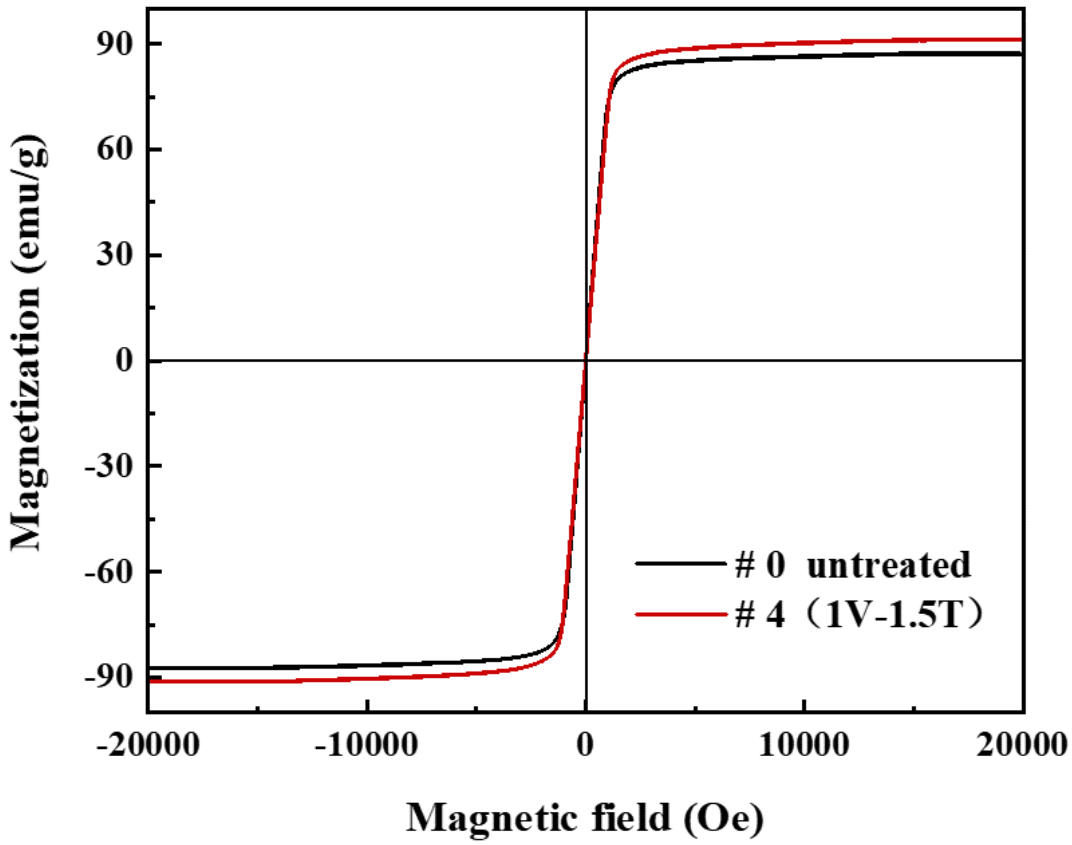

Fig. 5 B-H hysteresis loop of EP-13 Mn-Zn ferrites at ±2T after CEMT

Table 3 Saturation magnetization intensity (Ms) and the coercivity (Hc) of EP-13 Mn-Zn ferrites after CEMT

Sample number	Ms (emu/g)	Hc (Oe)
#0	87.09	4.92
#4	91.12	3.96

Fig. 5 shows the B-H hysteresis loop of the untreated sample (#0) and the sample after CEMT (#4). It can be seen in the figure that the hysteresis loop of EP-13 manganese zinc ferrite before and after CEMT is narrow and exhibits obvious soft magnetic material characteristics [1]. According to the data in Table 3, after CEMT with the optimal parameters, the sample's coercivity of the sample decreased by 19.51% and the saturation magnetization increased by 4.63%. In Mn-Zn ferrite, coercivity (Hc) and permeability (μ_i) are interrelated: lower coercivity generally reflects reduced resistance to domain wall motion and rotation, which in turn results in higher permeability. After treatment, the observed reduction in coercivity indicates facilitated domain wall motion, thereby contributing to the improvement in permeability [9].

3.2 Microstructure and elemental distribution

Fig. 6 shows the XRD images of the untreated (#0) and optimal parameter CEMT samples (#4). From Fig. 6(a), it can be observed that sample #4 exhibits a spinel phase, with clear and consistent characteristic peaks. There is no significant difference in crystal integrity compared to the untreated sample. The chemical formula is ($Mn_{0.64}Zn_{0.29}Fe_{2.07}O_4$), indicating that the original spinel structure of the Mn-Zn ferrite remains intact before and after the coupled electromagnetic treatment. To further study the influence of CEMT on the crystal structure of the samples, Rietveld analysis of the XRD patterns was conducted using Jade 6. The refined XRD patterns are presented in Fig. 6(b) and (c). As shown in Table 4, the fitting parameters (Rwp, Rp, and χ^2) are relatively low, indicating that the refinement results are within a reliable and acceptable range [11]. The lattice constant of the Mn-Zn ferrite increased slightly by approximately 0.05% after treatment. The unchanged diffraction peak positions confirm that the phase composition did not change. The increase in peak intensity indicates better lattice ordering and fewer microstructural defects. These changes may help improve the magnetic properties. The lattice parameter (a) was calculated by Bragg's formula from the strongest peak (311) [16].

$$a=\sqrt{h^2+k^2+l^2} \quad (3)$$

where, d_{hkl} is spacing value of (311).

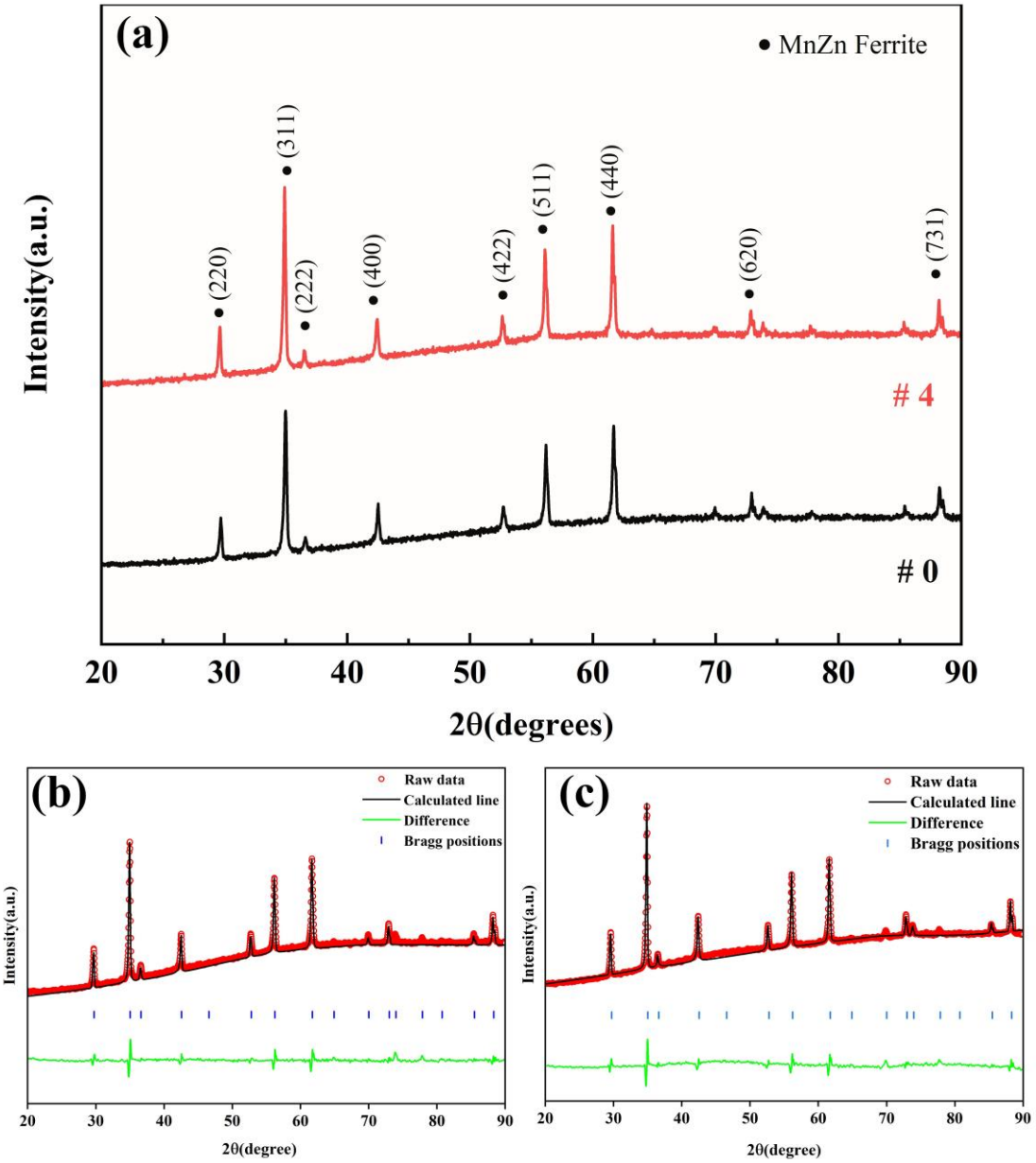

Fig. 6 XRD pattern of EP-13 Mn-Zn ferrites: (a) XRD patterns of the respective samples; (b) Rietveld-refined XRD patterns for #0; (c) Rietveld-refined XRD patterns for #4

Table 4 Refined structural parameters of Mn-Zn ferrites

Sample number	a(Å)	Rp (%)	Rwp (%)	χ2
#0	8.482	1.45	2.14	2.17
#4	8.487	2.11	2.92	1.92

Fig. 7 presents the SEM and BSE images of EP-13 Mn-Zn ferrite at various magnifications. In the untreated sample (Fig. 7(a)), the dominant fracture mode is intergranular, as indicated by the yellow dashed line separating intergranular and

transgranular regions. In contrast, after CEMT (Fig. 7(d)), transgranular fracture becomes the main mode, with only a few intergranular fractures remaining. The BSE images in Figs. 7(b) and (e) further supports this distinction. In the untreated sample, transgranular fractures are more numerous and clustered, while in the sample after CEMT, they are fewer and more dispersed. Additionally, magnified grain boundary images (Figs. 7(c) and (f)) show that the treatment results in more well-defined grain boundaries, reduced grain spacing, and enhanced intergranular bonding.

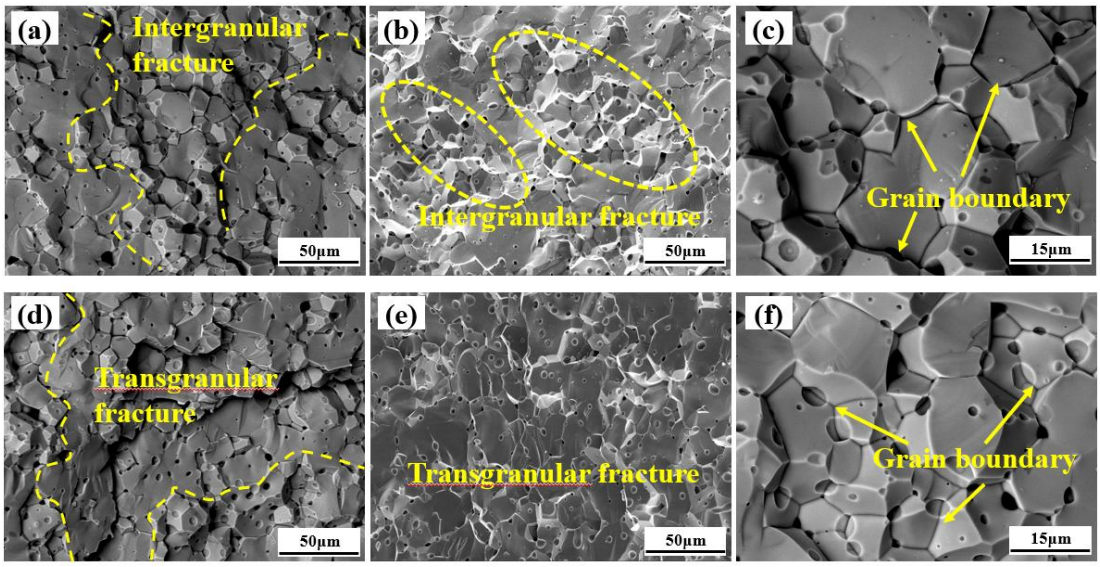

Fig. 7 SEM and BSE micrographs of samples: (a) SEM image of specimen #0, (b) BSE image specimen #0, (c) Grain boundary image of specimen #0, (d) SEM image of specimen #4, (e) BSE image of specimen #4, (f) Grain boundary image of specimen #4

The magnetization process in low and vanishing-anisotropy soft magnetic materials (e.g., soft ferrites and nanocrystalline ribbons, etc.) is usually shared by the rotation of the spins inside the domains and the motion of the domain walls [4]. Although these two mechanisms coexist, their relative contributions depend on the microstructural features of the material. When the grain size of Mn-Zn ferrite is large and there are fewer pores, the magnetization mechanism is mainly reversible domain wall motion. However, when the grain size of manganese zinc ferrite is small, there are more pores, and the internal structure is uneven, the resistance to domain wall motion increases, and reversible domain rotation becomes the main magnetization mechanism [31]. Specifically, the mobility of domain walls is strongly influenced by pinning and depinning processes. Pores, grain boundaries, and secondary phases act as pinning centers that hinder domain wall motion, increasing coercivity and magnetic losses. Kasahara et al. [32] provided direct in situ evidence using Lorentz microscopy and electron holography that domain walls in Mn-Zn and Ni-Zn ferrites are strongly pinned

at grain boundaries and pores, and depinning occurs only when the local magnetic field is sufficient to overcome the associated energy barriers. Similarly, Sun et al. [33] demonstrated that ZrO_2 precipitation and agglomeration in Mn-Zn ferrites introduce additional pinning sites, significantly suppressing domain wall mobility and deteriorating soft magnetic properties. In this study, CEMT reduces internal defects and promotes the transformation of low-angle grain boundaries into high-angle ones, thereby decreasing both the number and effectiveness of pinning centers. This microstructural refinement enables smoother domain wall motion under a magnetic field, reducing resistance to both wall motion and spin rotation during magnetization. This enhances the ferrite core's magnetic performance and improves its reliability [34].

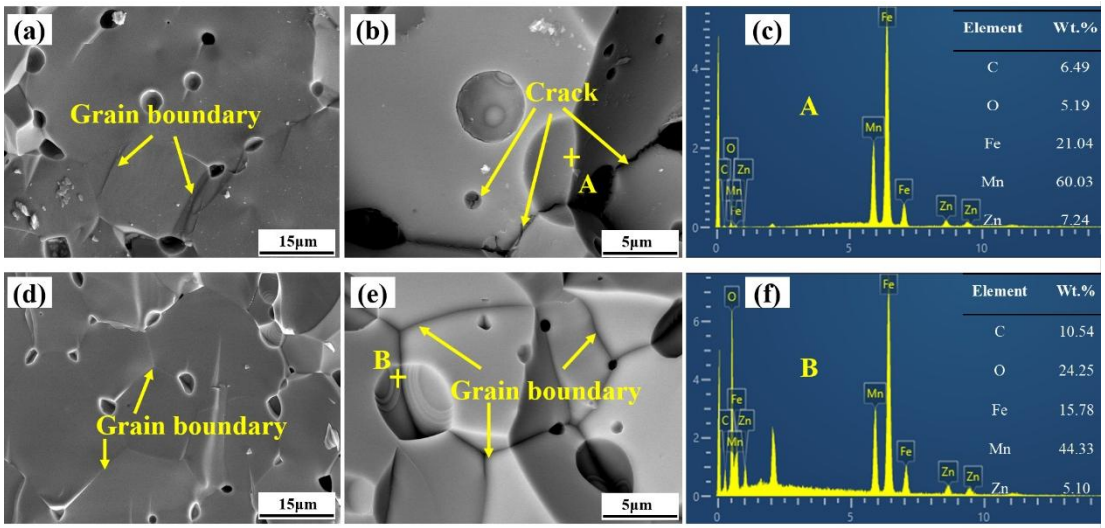

Fig. 8 SEM and EDS micrographs of samples: (a) SEM image of transgranular fracture area of specimen #0, (b) SEM image of intergranular fracture area of specimen #0, (c) EDS at grain boundary of specimen #0, (d) SEM image of transgranular fracture area of specimen #4, (e) SEM image of intergranular fracture area of specimen #4, (f) EDS at grain boundary image of specimen #4

Fig. 8 shows a comparative analysis of the transgranular fracture regions in both the untreated specimen (#0) and the specimen after CEMT (#4). In specimen #0, microscopic defects such as cracks are clearly visible at and near the grain boundaries. These defects act as initiation sites for damage initiation and propagation under external forces, ultimately causing failure. Moreover, these grain boundary defects can pin domain walls, increasing the energy loss during domain wall motion, which in turn raises coercivity and leads to higher power loss [35]. Conversely, the cross-section of the transgranular fracture area in samples (#4) shows a cleaner fracture surface with well-defined grain boundaries and reduced grain boundary spacing. EDS analysis of the grain boundaries indicates an increase in oxygen elements and a decrease in other

elements in sample (#4). This observation is attributed to the CEMT repairs small defects at the grain boundaries. The modified local chemical environment likely enhances grain boundary cohesion. During this repair, the accumulation of strengthening elements at the boundaries may enhance intergranular bonding strength. Such changes could be associated with the formation of a less conductive grain boundary region, which may hinder localized eddy current formation and thereby contribute to a reduction in eddy current losses. Simultaneously, the CEMT process induces residual compressive stress due to the magnetostriction effect and dislocation movements, counteracting tensile residual stress from prior manufacturing processes. This redistribution of stress reduces internal resistance to domain wall motion, thereby lowering power loss and improving permeability [36].

3.3 EBSD observation

Fig. 9 presents the quasi-in-situ EBSD results of EP-13 Mn-Zn power ferrite before and after CEMT. Figs. 9(a) and (b) show the distribution maps of Euler angles, while Figs. 9(c) and (d) display the corresponding IPF maps. The colors of different grains represent their different crystallographic orientation angles. The same regions before and after treatment are marked by corresponding yellow dashed lines labeled 1, 2, and 3 in Figs. 9(a) and (b), and by black dashed lines labeled 1 and 2 in Figs. 9(c) and (d), respectively. This phenomenon suggests that the combined effect of pulsed current and electromagnetic fields induced some grains of the Mn-Zn ferrite to change their crystal orientation. The change can be attributed to the reduction of dislocation pinning, which allowed dislocations to slip and climb more easily, thereby altering grain orientation. Additionally, the magnetostriction effect from the alternating magnetic field may have introduced local lattice distortions, further facilitating orientation adjustment [37]. The changes observed in the deformed regions of the Euler angle and IPF maps also indicate that CEMT may have contributed to the release of residual stress. Samples before treatment likely exhibited high internal stress and non-uniform grain orientations, whereas treated samples showed a more uniform crystallographic distribution. These microstructural modifications can influence domain wall motion, thereby enhancing the initial permeability and reducing magnetic loss. Moreover, the relaxation of internal stress is expected to improve the stability and long-term service performance of ferrite materials [38].

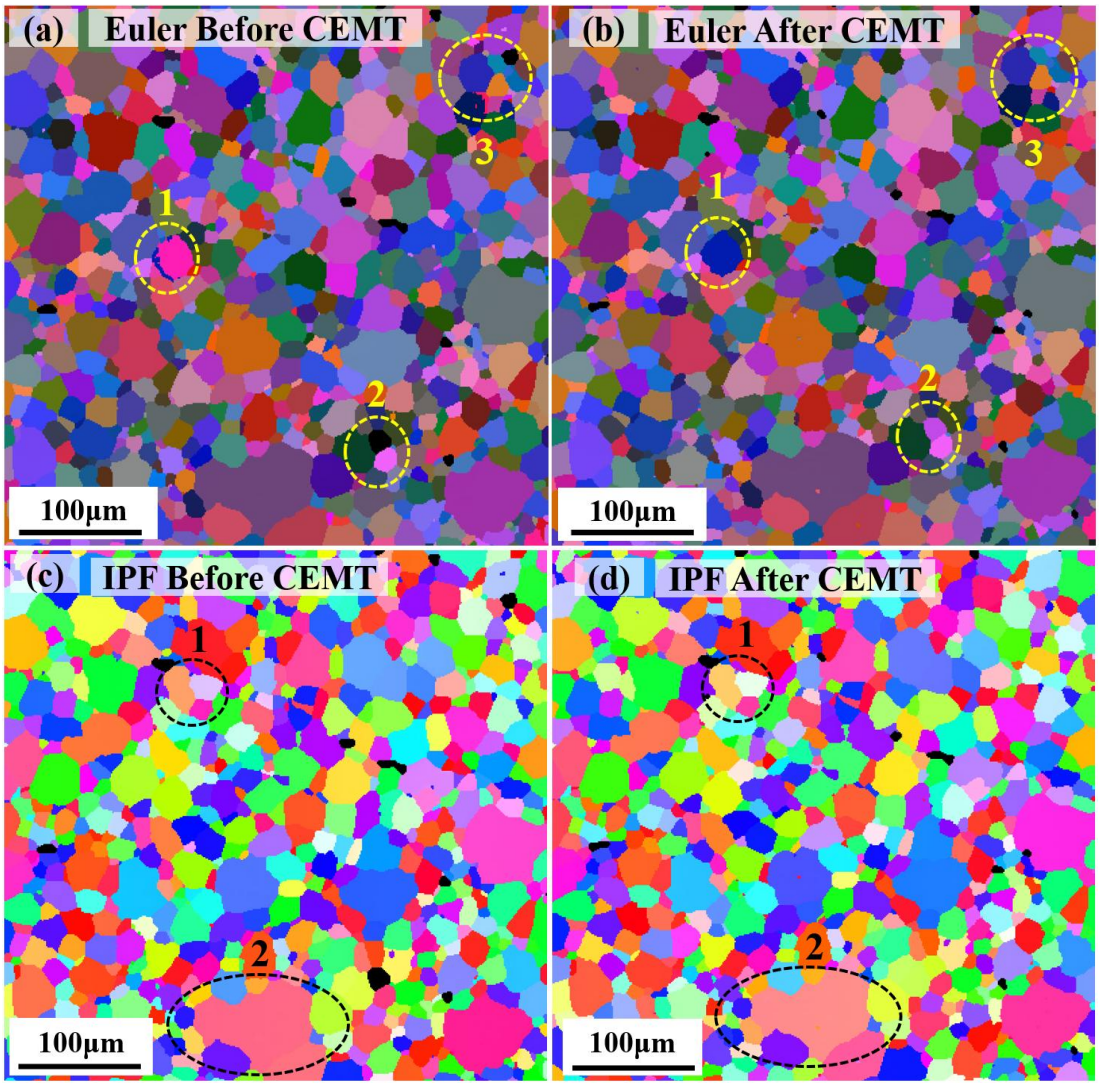

Fig. 9 EBSD images of EP-13 Mn–Zn ferrite before and after CEMT: (a) before CEMT, (b) after CEMT, (c) IPF map before CEMT, (b) IPF map after CEMT

In summary, the results indicate that CEMT influenced the crystallographic orientation of Mn-Zn ferrite and may positively affect its magnetic properties by regulating dislocation behavior and residual stress distribution. Further analysis, including KAM (Kernel Average Misorientation) mapping and grain boundary angle statistics, will provide deeper insights into the relationship between microstructural evolution and magnetic property optimization.

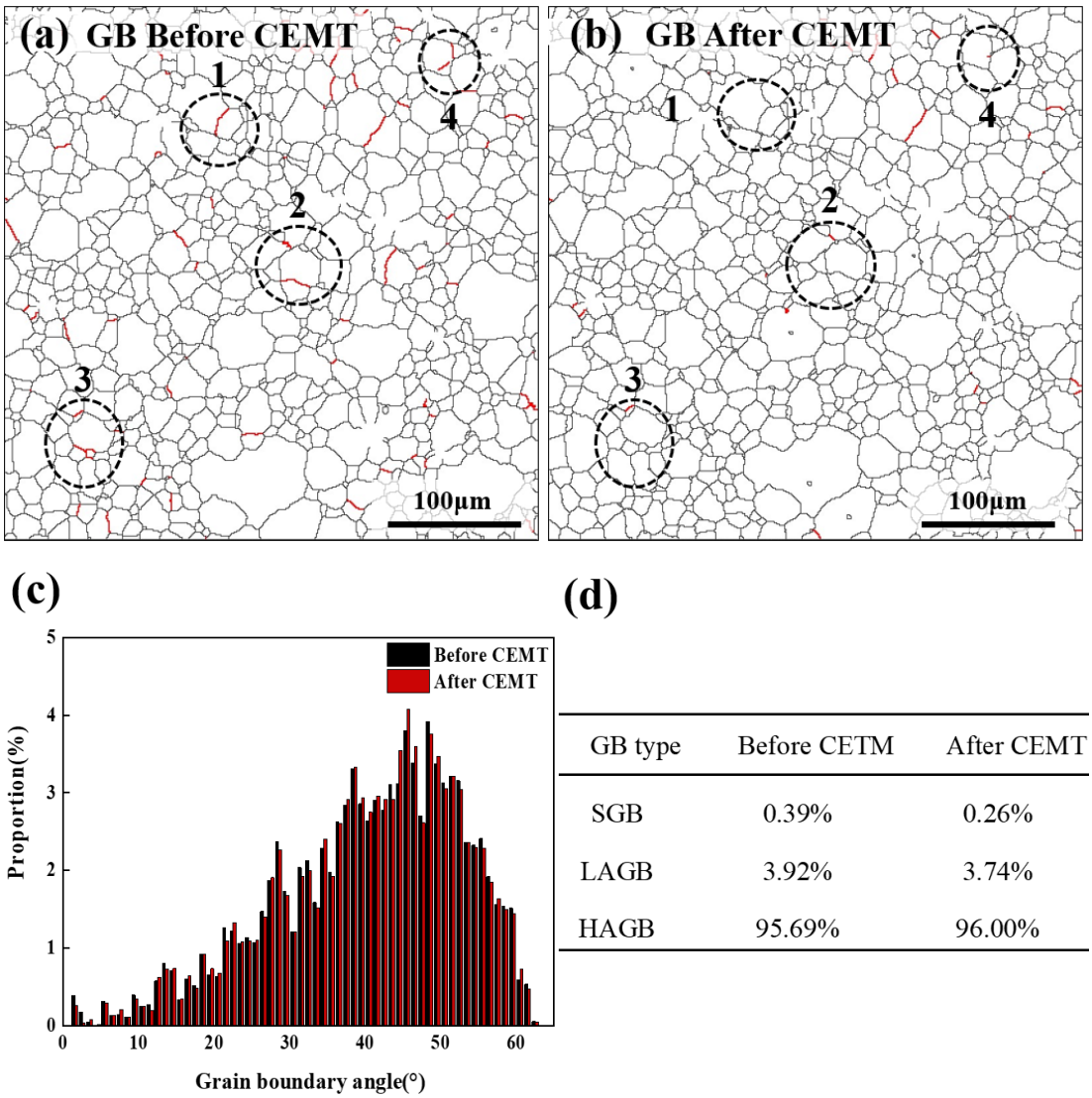

GB type	Before CETM	After CEMT
SGB	0.39%	0.26%
LAGB	3.92%	3.74%
HAGB	95.69%	96.00%

Fig. 10 GB map of EP-13 Mn–Zn ferrite before and after CEMT: (a) before CEMT, (b) after CEMT, (c) grain boundary angle statistical diagram, (d) statistical table of grain boundary angle content.

Fig. 10 illustrates the grain boundary (GB) maps of the EP-13 Mn-Zn ferrites before and after CEMT with quasi-in-situ EBSD. Figs. 10(a) and 10(b) represent the grain boundary angle distribution before and after treatment, with four regions showing noticeable changes marked by black dashed lines and labeled as 1 to 4 in each image. Fig. 10(c) provides a statistical distribution of grain boundary angles, and Fig. 10(d) summarizes the proportions of different grain boundary angle categories. It is evident from the images that the number of small-angle grain boundaries (SGB, 0–2°) and low-angle grain boundaries (LAGB, 2–15°) decreases in the treated sample, while the proportion of high-angle grain boundaries (HAGB, >15°) increases. Notably, the red-marked SGBs in Fig. 10(b) are visibly fewer than those in Fig. 10(a), indicating that CEMT significantly influenced grain boundary evolution. Further statistical analysis

shows that before CEMT, the SGB content was 0.39%, the LAGB content was 3.92%, and the HAGB content was 95.69%. After treatment, the SGB content decreased to 0.26%, the LAGB content decreased to 3.74%, and the HAGB content increased to 96.00%. This trend suggests that CEMT facilitates the transformation of low-angle grain boundaries to high-angle grain boundaries, which is likely related to dislocation rearrangement, migration, and the release of residual stress [39]. Combining the analysis from Fig. 9, the grain boundary evolution further supports the occurrence of microstructural reorganization. Dislocation theory suggests that the LAGBs primarily consist of dislocation concentration, and a higher LAGB content implies the presence of more dislocations and stress concentration within the grains [40]. The observed increase in HAGBs implies reduced dislocation density and internal stress. This transformation can weaken the pinning effect on magnetic domain walls, lowering the resistance to domain wall motion and rotation. As a result, the initial permeability of the Mn-Zn ferrite is enhanced, and magnetic losses are reduced. It is also noteworthy that, considering the high resistivity of Mn-Zn ferrite and the low applied electric field (1V), the theoretical Joule heating during CEMT is minimal, and no significant temperature rise was observed in practice. This further confirms that the microstructural changes, such as grain boundary evolution and orientation adjustment, are dominated by field-assisted mechanisms rather than thermal effects.

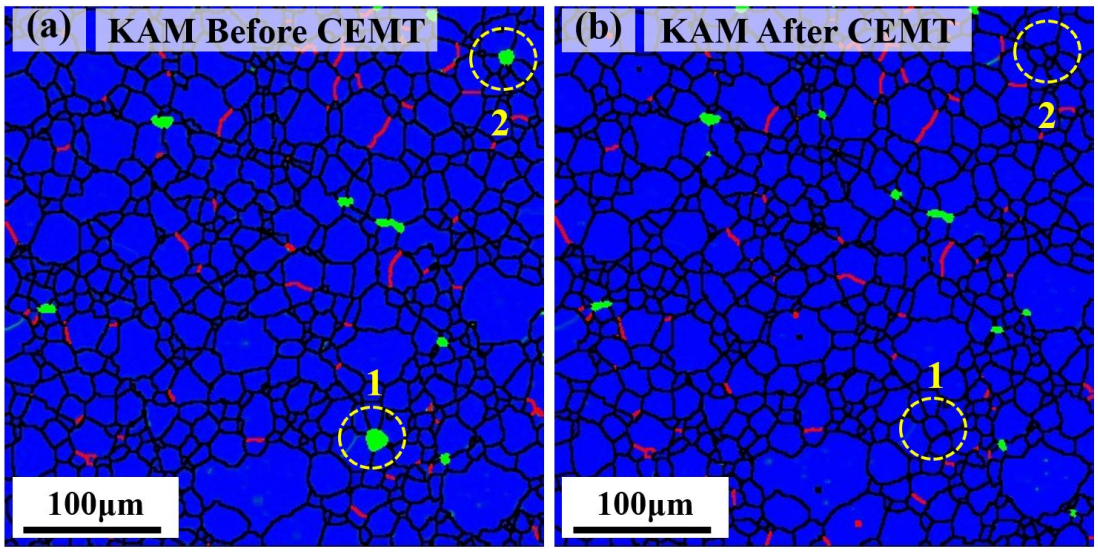

Fig. 11 KAM map of EP-13 Mn–Zn ferrite before and after CEMT: (a) before CEMT, (b) after CEMT

These microstructural optimizations may positively influence the enhancement of magnetic properties. Further KAM analysis can help reveal the relationship between

dislocation density changes and the optimization of magnetic performance. Previous studies have demonstrated that KAM can be used to qualitatively characterize changes in the true dislocation density [41]. To explore the relationship between the crystal orientation, change and dislocation movement, the following formulas are used to calculate the geometrically necessary dislocation (GND) density in the specimens:

$$\rho_{GND}=\frac{2\theta}{\mu b} \tag{4}$$

where ρ_{GND} represents geometrically necessary dislocation density, θ is the mean value of the kernel averaged misorientation in the selected area, μ is the scanning step size, b is the Burgers vector.

Fig. 11 presents the Kernel Average Misorientation (KAM) maps obtained through quasi-in-situ EBSD before and after CEMT. Specifically, Figure 11(a) represents the untreated state, while Figure 11(b) depicts the state after treatment. A clear reduction in dislocation density can be observed in the treated sample, particularly in areas 1, 2, and 3. Table 5 provides the statistical data for the average KAM values and geometric dislocation density. Before treatment, the average misorientation angle (KAM value) was 0.3571, which decreased to 0.2083 after treatment. The dislocation density was 1.701 before treatment and decreased to 0.992 after treatment.

Table 5 Mean value of KAM and geometric dislocation density of Mn-Zn ferrite

GB type	$\theta/°$	$\rho_{GND}/10^{15}m^2$
Before CEMT	0.3571	1.701
After CEMT	0.2083	0.992

The KAM maps (Fig. 11) and statistical data in Table 4 indicate a noticeable reduction in dislocation density after CEMT. This change aligns with the observed decrease in low-angle grain boundaries (LAGBs) in Fig. 10, suggesting that CEMT facilitates dislocation movement and annihilation. These processes not only refine the microstructure but also relieve internal stress concentrations, which are beneficial for enhancing magnetic performance and reducing energy loss [42]. The KAM analysis results of this study indicate that the dislocation density of the specimens decreased by approximately 41.7% after CEMT, while the proportion of low-angle grain boundaries (LAGBs) decreased by 4.6%. These microstructural changes imply that residual stress has been released, the number of domain wall pinning points has decreased, and the obstacles to domain wall movement have been reduced. Correspondingly, magnetic property test results indicate that the coercivity decreased by 19.51%. Since the initial

permeability (μ_i) is inversely proportional to the coercivity (Hc), the initial permeability increased by 10.09% and 5.58% at 25°C and 100°C, respectively. This correspondence between microstructural optimization and macroscopic performance improvement indicates that CEMT plays a direct structural regulatory role in enhancing the magnetic properties of ferrites.

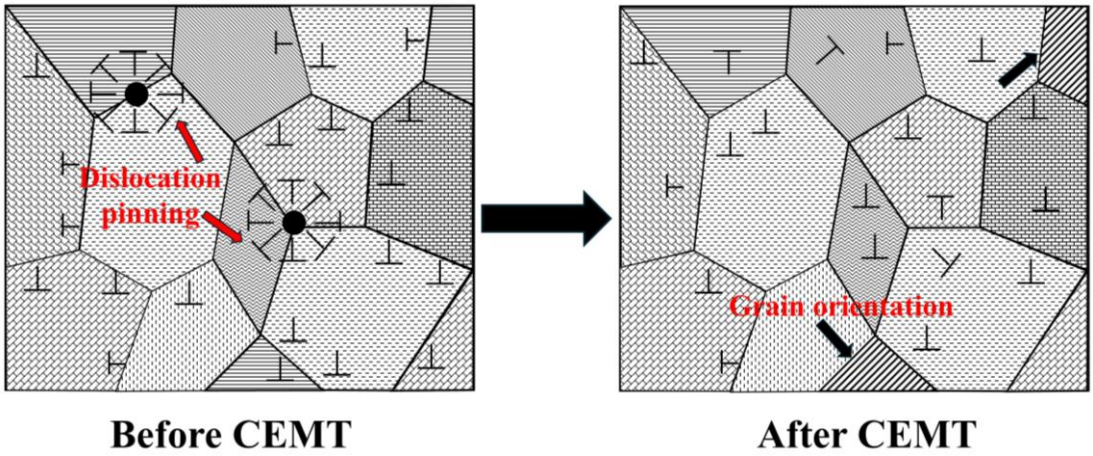

Fig. 12 Schematic diagram of the mechanism of EMCT

This microstructural evolution results from the synergistic effects of pulsed electric and magnetic fields. The pulsed current drives charge redistribution and defect mitigation, while the alternating magnetic field induces magnetostrictive strain that enables crystallographic reorientation and reduces lattice distortions. As a result, both dislocation density and residual stress are reduced, and domain walls can move more easily, leading to improved permeability and lower energy loss. This explanation is supported by prior studies. Shipko et al. [43] demonstrated that pulsed magnetic fields can alter the distribution of cation vacancies and relax local lattice distortions, effectively reducing internal stress concentrations. Alshits et al. [29] further reported that electric fields can drive dislocation motion through localized charge effects and electron wind forces, enabling dislocation glide and annihilation.

Fig. 12 offers a schematic representation of microstructural change during CEMT. Before treatment, dislocations (T-shaped symbols) are pinned at defects and grain boundaries (black circles), where they accumulate and act as obstacles to domain wall motion. After CEMT, dislocation motion and annihilation are facilitated, resulting in fewer pinning sites and a lower overall dislocation density. The grains are filled with different patterns to indicate their crystallographic orientations, while the changes highlighted by black arrows illustrate grain reorientation induced by the treatment. These combined effects reduce obstacles to domain wall motion, enabling permeability

enhancement and energy loss reduction. Notably, excessive field intensities may induce additional microplastic deformation, indicating the need to optimize CEMT parameters to balance performance enhancement and microstructural stability.

In summary, CEMT effectively affects the crystal orientation of Mn-Zn ferrite (Fig. 9) and promotes the evolution of grain boundaries evolution (Fig. 10), particularly by reducing LAGBs that act as a barrier to domain wall motion. These microstructural improvements are supported by KAM analysis (Fig. 11), which demonstrates the release of residual stress and optimization of dislocation structures. Compared to traditional methods, CEMT provides a novel, non-chemical pathway for improving Mn-Zn ferrite performance through microstructure-driven magnetic regulation. In this study, the EP-13 Mn-Zn ferrite employed was a widely used commercial product rather than a laboratory-specific sample. Our results demonstrate an increase in permeability and a reduction in power loss, corresponding to an estimated 5-7% improvement in energy efficiency for transformer cores under high-frequency operation relative to untreated commercial products. This study has verified the feasibility of using CEMT to improve the magnetic properties of Mn-Zn ferrites, and future work will extend this approach to device-level validation and scaling up for more complex core geometries.

4. Conclusions

To address the need for improved magnetic performance and reduced power loss in Mn-Zn ferrites, this study applied a novel coupled electromagnetic treatment (CEMT) to EP-13 Mn-Zn ferrite. The effects of different processing parameters were systematically investigated, and the resulting magnetic properties were analyzed. The main conclusions are as follows:

(1) CEMT effectively enhances the magnetic properties of Mn-Zn ferrite. Initial permeability and power loss exhibited notable variations under different CEMT conditions. The variation trend indicates that the optimization of electromagnetic field parameters directly influences these properties.

(2) Under the optimal CEMT parameters (magnetic field strength of 1.5T and electric field intensity of 1V), the initial permeability increased by 10.09% at 25℃ and by 5.58% at 100°C. The power loss was reduced by 2.80% at 25℃ and by 6.81% at 100°C. Additionally, the coercivity decreased by 19.51%, and the saturation

magnetization increased by 4.63%.

(3) The CEMT facilitates grain reorientation, reduces the proportion of low-angle grain boundaries (LAGBs), and promotes the dislocations rearrangement and annihilation. These microstructural changes lead to a more ordered grain structure and contribute to the relaxation of residual stress within the ferrite. As a result, magnetic domain wall motion encounters less resistance during magnetization, thereby enhancing domain wall mobility and reducing overall energy loss.

(4) CEMT is a promising and environmentally friendly technique for optimizing soft magnetic materials. It supports real-time parameter adjustment during processing, making it more flexible and potentially scalable for industrial applications. This study provides a foundation for the application of CEMT in improving the performance of Mn-Zn ferrites, demonstrating its potential for next-generation power ferrite applications. Future research will focus on refining treatment parameters and exploring its applicability to other soft magnetic materials.

(5) Future work should focus on scaling up CEMT to complex ferrite core geometries and evaluating its long-term stability under thermal cycling and magnetic aging conditions. Such efforts will be critical to verifying the industrial applicability of CEMT and ensuring the durability of its magnetic property enhancements in high-frequency power electronic devices.

Acknowledgement

The authors wish to acknowledge the financial support by the Science Foundation of Luzhou Government and Sichuan University, China (No. 2022CDLZ-14). We would like to appreciate the Analytical and Testing Center of Sichuan University for structural characterization work.

References

[1] J.M. Silveyra, E. Ferrara, D.L. Huber, T.C. Monson, Soft magnetic materials for a sustainable and electrified world, Science 362 (2018) 418. https://doi.org/10.1126/science.aao0195.

[2] P. Andalib, V.G. Harris, Grain boundary engineering of power inductor cores for MHz applications, J. Alloy. Compd. 832 (2020) 153131. https://doi.org/10.1016/j.jallcom.2019.153131.

[3] A. Krings, A. Boglietti, A. Cavagnino, S. Sprague, Soft Magnetic Material Status and Trends in Electric Machines, IEEE Trans. Ind. Electron. 64 (2017) 2405-2414. https://doi.org/10.1109/TIE.2016.2613844.

[4] V. Tsakaloudi, C. Beatrice, F. Fiorillo, V. Zaspalis, Magnetic loss versus temperature and role of doping in Mn-Zn ferrites, J. Magn. Magn. Mater. 603 (2024) 172228. https://doi.org/10.1016/j.jmmm.2024.172228.

[5] P. Thakur, D. Chahar, S. Taneja, N. Bhalla, A. Thakur, A review on MnZn ferrites: Synthesis , characterization and applications, Ceram. Int. 46 (2020) 15740-15763. https://doi.org/10.1016/j.ceramint.2020.03.287.

[6] R. Guo, X. Yang, K. Sun, K. Li, Z. Yu, G. Wu, X. Zhang, X. Jiang, Z. Lan, Temperature characteristics of core losses for HfO2 doped manganese-zinc ferrites, J. Magn. Magn. Mater. 491 (2019) 165554. https://doi.org/10.1016/j.jmmm.2019.165554.

[7] C.A. Baguley, U.K. Madawala, B. Carsten, The Influence of Remanence on Magnetostrictive Vibration and Hysteresis in Mn-Zn Ferrite Cores, IEEE Trans. Magn. 48 (2012) 1844-1850. https://doi.org/10.1109/TMAG.2011.2174251.

[8] C. Beatrice, V. Tsakaloudi, S. Dobák, V. Zaspalis, F. Fiorillo, Magnetic losses versus sintering treatment in Mn-Zn ferrites, J. Magn. Magn. Mater. 429 (2017) 129-137. https://doi.org/10.1016/j.jmmm.2016.12.121.

[9] Q. Xing, Z. Peng, C. Wang, Z. Fu, X. Fu, Doping effect of Y3+ ions on the microstructural and electromagnetic properties of Mn–Zn ferrites, Physica B 407 (2012) 388-392. https://doi.org/10.1016/j.physb.2011.11.003.

[10] A. Hussain, G. Bai, H. Huo, S. Yi, X. Wang, X. Fan, M. Yan, Co2O3 and SnO2 doped MnZn ferrites for applications at 3-5 MHz frequencies, Ceram. Int. 45 (2019) 12544-12549. https://doi.org/10.1016/j.ceramint.2019.03.193.

[11] X. Ji, C. Shen, Y. Zhao, H. Zheng, Q. Wu, Q. Zhang, L. Zheng, P. Zheng, Y. Zhang, Enhanced electromagnetic properties of low-temperature sintered NiCuZn ferrites by doping with Bi2O3, Ceram. Int. 48 (2022) 20315-20323. https://doi.org/10.1016/j.ceramint.2022.03.313.

[12] G. Kogias, V.T. Zaspalis, Temperature stable MnZn ferrites for applications in the frequency region of 500 kHz, Ceram. Int. 42 (2016) 7639-7646. https://doi.org/10.1016/j.ceramint.2016.01.176.

[13] H. Li, J. Wang, S. Lv, C. Chen, H. Luo, Q. Wu, Q. Zhang, H. Zheng, L. Zheng, Curie temperature and magnetic permeability regulation of Cr–Mg co-doped NiCuZn ferrite for tumor hyperthermia, Ceram. Int. 50 (2024) 25925-25932. https://doi.org/10.1016/j.ceramint.2024.04.335.

[14] S.V. Bhandare, R. Kumar, A.V. Anupama, H.K. Choudhary, V.M. Jali, B. Sahoo, Mechanistic insights into the sol-gel synthesis of complex (quaternary) Co–Mn–Zn-spinel ferrites: An annealing dependent study, Ceram. Int. 46 (2020) 17400-17415. https://doi.org/https://doi.org/10.1016/j.ceramint.2020.04.031.

[15] Y. Ying, L. Hu, Z. Li, J. Zheng, J. Yu, W. Li, L. Qiao, W. Cai, J. Li, D. Bao, S. Che, Preparation of Densified Fine-Grain High-Frequency MnZn Ferrite Using the Cold Sintering Process, Materials 16 (2023) 3454. https://doi.org/10.3390/ma16093454.

[16] X. Zhou, J. Wang, L. Zhou, Y. Wang, D. Yao, Structure, magnetic and microwave absorption properties of NiZnMn ferrite ceramics, J. Magn. Magn. Mater. 534 (2021) 168043. https://doi.org/https://doi.org/10.1016/j.jmmm.2021.168043.

[17] H. Li, L.F. Peng, B. Meng, Z.T. Xu, L.L. Wang, G. Ngaile, M.W. Fu, Energy field assisted metal forming: Current status, challenges and prospects, Int. J. Mach. Tools Manuf. 192 (2023) 104075. https://doi.org/10.1016/j.ijmachtools.2023.104075.

[18] B.E. Klamecki, Residual stress reduction by pulsed magnetic treatment, J. Mater. Process. Technol. 141 (2003) 385-394. https://doi.org/10.1016/S0924-0136(03)00387-X.

[19] L. Pan, W. He, B. Gu, Effects of electric current pulses on mechanical properties and microstructures of as-quenched medium carbon steel, Mater. Sci. Eng. A-Struct. Mater. Prop. Microstruct. Process. 662 (2016) 404-411. https://doi.org/10.1016/j.msea.2016.03.031.

[20] M.N. Shipko, V.V. Korovushkin, V.G. Kostishin, I.M. Isaev, M.A. Stepovich, E.S. Savchenko, Effect of Magnetic Pulse Processing on the Structure and Magnetic Properties of Ferrites, Bulletin of the Russian Academy of Sciences. Physics 82 (2018) 203-207. https://doi.org/10.3103/S1062873818020235.

[21] Z. Cai, X. Huang, Residual stress reduction by combined treatment of pulsed magnetic field and pulsed current, Materials Science and Engineering: A 528 (2011) 6287-6292. https://doi.org/10.1016/j.msea.2011.04.078.
[22] L. Ashi, Z. Xie, H. Sun, J. Wang, K. Huang, Effect of electromagnetic coupling treatment on the residual stress relief and mechanical properties of 7050 aluminum alloy, J. Mater. Sci. 58 (2023) 12097-12117. https://doi.org/10.1007/s10853-023-08775-y.
[23] Q. Zhang, X. Wang, Y. Qin, G. He, S. Zhang, K. Huang, J. Wang, Improving thermal conductivity of a nickel-based alloy through advanced electromagnetic coupling treatment, J. Mater. Res. Technol-JMRT 21 (2022) 4708-4723. https://doi.org/10.1016/j.jmrt.2022.11.066.
[24] Q. Li, X. Wang, Y. Qin, K. Huang, J. Wang, Improvement of the fatigue life of an electron-beam welded Ti2AlNb joint subjected to an electromagnetic coupling treatment, Mater. Sci. Eng. A-Struct. Mater. Prop. Microstruct. Process. 909 (2024) 146848. https://doi.org/10.1016/j.msea.2024.146848.
[25] C. Liang, K. Lin, The microstructure and property variations of metals induced by electric current treatment: A review, Mater. Charact. 145 (2018) 545-555. https://doi.org/10.1016/j.matchar.2018.08.058.
[26] Y. Yang, Y. Yang, Q. Li, Y. Qin, G. Yang, B. Zhou, C. Deng, M. Wu, An eco-friendly pulsed magnetic field treatment on cemented carbide (WC–12Co) for enhanced milling performance, J. Clean Prod. 340 (2022) 130748. https://doi.org/10.1016/j.jclepro.2022.130748.
[27] M. Yuan, J. Wang, L. Wang, F. Zhong, K. Huang, Y. Tian, Electromagnetic coupling field strengthening of WC-TiC-Co cermet tools, Ceram. Int. 47 (2021) 3747-3759. https://doi.org/10.1016/j.ceramint.2020.09.232.
[28] H. Sun, L. Zhang, Y. Wang, Y. Qin, Z. Xie, L. Ashi, N. Xu, K. Huang, J. Wang, J. Huang, Improving fatigue life of a titanium alloy through coupled electromagnetic treatments, Int. J. Fatigue 191 (2025) 108676. https://doi.org/10.1016/j.ijfatigue.2024.108676.
[29] M. Li, Y. Shen, K. Luo, Q. An, P. Gao, P. Xiao, Y. Zou, Harnessing dislocation motion using an electric field, Nat. Mater. 22 (2023) 958-963. https://doi.org/10.1038/s41563-023-01572-7.
[30] K. Sun, Z. Lan, Z. Yu, Z. Xu, X. Jiang, Z. Wang, Z. Liu, M. Luo, Temperature and frequency characteristics of low-loss MnZn ferrite in a wide temperature range, J. Appl. Phys. 109 (2011) 106103. https://doi.org/10.1063/1.3583551.
[31] X. Ji, T. Chen, C. Shen, Y. Zhao, K. Zhou, M. Sun, Y. Yu, L. Fan, H. Zheng, Q. Wu, Q. Zhang, Y. Zhang, Magnetic and dielectric properties of NiCuZn ferrite with optimized Cu content and sintered by a two-step process, J. Alloy. Compd. 898 (2022) 162906. https://doi.org/10.1016/j.jallcom.2021.162906.
[32] T. Kasahara, H.S. Park, D. Shindo, H. Yoshikawa, T. Sato, K. Kondo, In situ observations of domain wall motion in Mn–Zn and Ni–Zn ferrites by Lorentz microscopy and electron holography, J. Magn. Magn. Mater. 305 (2006) 165-170. https://doi.org/10.1016/j.jmmm.2005.12.007.
[33] B. Sun, F. Chen, D. Xie, W. Yang, H. Shen, A large domain wall pinning effect on the magnetic properties of ZrO2 added Mn–Zn ferrites, Ceram. Int. 40 (2014) 6351-6354. https://doi.org/10.1016/j.ceramint.2013.10.127.
[34] Z. Li, Y. Ying, N. Wang, J. Zheng, J. Yu, W. Li, L. Qiao, W. Cai, J. Li, H. Huang, Y. Liu, T. Zhao, S. Che, Effect of compressive stress on power loss of Mn–Zn ferrite for high-frequency applications, Ceram. Int. 48 (2022) 17723-17728. https://doi.org/10.1016/j.ceramint.2022.03.042.
[35] T. Hasegawa, S. Kanatani, M. Kazaana, K. Takahashi, K. Kumagai, M. Hirao, S. Ishio, Conversion of FeCo from soft to hard magnetic material by lattice engineering and nanopatterning, Sci Rep 7 (2017) 13215. https://doi.org/10.1038/s41598-017-13602-x.
[36] V. Tsakaloudi, D. Holz, V. Zaspalis, The effect of externally applied uniaxial compressive stress on the magnetic properties of power MnZn-ferrites, J. Mater. Sci. 48 (2013) 3825-3833. https://doi.org/10.1007/s10853-013-7183-2.
[37] Q. Shao, J.J. Kang, Z.G. Xing, H.D. Wang, Y.F. Huang, G.Z. Ma, H.P. Liu, Effect of pulsed magnetic field treatment on the residual stress of 20Cr2Ni4A steel, J. Magn. Magn. Mater. 476 (2019) 218-224. https://doi.org/10.1016/j.jmmm.2018.12.105.
[38] G. Huang, R. Liu, S. Hu, Investigation of the mechanism for reduction of residual stress through magnetic-vibration stress relief treatment, J. Magn. Magn. Mater. 582 (2023) 171041. https://doi.org/10.1016/j.jmmm.2023.171041.
[39] B.E. Klamecki, Residual stress reduction by pulsed magnetic treatment, J. Mater. Process. Technol. 141 (2003) 385-394. https://doi.org/10.1016/S0924-0136(03)00387-X.
[40] B. Zeng, Z.Q. Xie, Q. Li, J. Wang, K.L. Huang, H. Yu, Residual Stress Relaxation of 2A02 Blade Forging Under Electromagnetic Coupling Energy, Rare Metal Mat. Eng. 52 (2023) 4055-4064.

https://doi.org/10.12442/j.issn.1002-185X.20230281.
[41] K. Fujiyama, K. Mori, D. Kaneko, H. Kimachi, T. Saito, R. Ishii, T. Hino, Creep damage assessment of 10Cr-1Mo-1W-VNbN steel forging through EBSD observation, Int. J. Pressure Vessels Pip. 86 (2009) 570-577. https://doi.org/10.1016/j.ijpvp.2009.04.011.
[42] G. Ananthakrishna, Current theoretical approaches to collective behavior of dislocations, Phys. Rep.-Rev. Sec. Phys. Lett. 440 (2007) 113-259. https://doi.org/10.1016/j.physrep.2006.10.003.
[43] M.N. Shipko, V.V. Korovushkin, V.G. Kostishin, I.M. Isaev, M.A. Stepovich, E.S. Savchenko, Effect of Magnetic Pulse Processing on the Structure and Magnetic Properties of Ferrites, Bulletin of the Russian Academy of Sciences. Physics 82 (2018) 203-207. https://doi.org/10.3103/S1062873818020235.